Optics Letters

Blind source separation with integrated photonics and reduced dimensional statistics

Philip Y. Ma,[1,*] Alexander N. Tait,[2] Weipeng Zhang,[1] Emir Ali Karahan,[1] Thomas Ferreira de Lima,[1] Chaoran Huang,[1] Bhavin J. Shastri,[3] and Paul R. Prucnal[1]

[1]Department of Electrical Engineering, Princeton University, Princeton, New Jersey 08544, USA
[2]Physical Measurement Laboratory, National Institute of Standards and Technology, Boulder, Colorado 80305, USA
[3]Department of Physics, Engineering Physics and Astronomy, Queen's University, Kingston, Ontario K7L 3N6, Canada
*Corresponding author: yechim@princeton.edu

Received 7 September 2020; revised 26 October 2020; accepted 29 October 2020; posted 29 October 2020 (Doc. ID 409474); published 30 November 2020

Microwave communications have witnessed an incipient proliferation of multi-antenna and opportunistic technologies in the wake of an ever-growing demand for spectrum resources, while facing increasingly difficult network management over widespread channel interference and heterogeneous wireless broadcasting. Radio frequency (RF) blind source separation (BSS) is a powerful technique for demixing mixtures of unknown signals with minimal assumptions, but relies on frequency dependent RF electronics and prior knowledge of the target frequency band. We propose photonic BSS with unparalleled frequency agility supported by the tremendous bandwidths of photonic channels and devices. Specifically, our approach adopts an RF photonic front-end to process RF signals at various frequency bands within the same array of integrated microring resonators, and implements a novel two-step photonic BSS pipeline to reconstruct source identities from the reduced dimensional statistics of front-end output. We verify the feasibility and robustness of our approach by performing the first proof-of-concept photonic BSS experiments on mixed-over-the-air RF signals across multiple frequency bands. The proposed technique lays the groundwork for further research in interference cancellation, radio communications, and photonic information processing.

https://doi.org/10.1364/OL.409474

The accelerating demands on spectrum resources are pushing radio operations into performance regimes that require more efficient spectrum utilizations [1]. Emerging opportunistic or coexistence solutions aim to address this problem by exploiting other degrees of freedom not in the spectral domain, while facing the challenge of providing satisfactory information assurance. For example, beamforming techniques may communicate with multiple users at the same frequency band given spatially distinct beam propagations [2], but suffer from inevitable interference among in-band sources at the reception end. Meanwhile, cognitive radio temporally allows secondary users to access unlicensed bands in the absence of its primary users [3], but requires an effective radio-signal identification mechanism to enforce wideband spectrum monitoring. Conventionally, these problems can be collectively framed in the context of blind source separation (BSS), aiming to achieve signal decomopsition with minimal knowledge on either source characteristics or the mixing process [4].

Radio frequency (RF) electronics have dominated for decades the front-end analog processing of wireless communication systems [5]; however, these technology platforms still present issues that make them not entirely suitable for handling BSS problems in the RF domain. One particular reason is that they are inherently frequency dependent, which results in limited reconfigurability in terms of both functional programmability and frequency agility [6]. In contrast, BSS solutions are not supposed to be aware of the target frequency band of incoming mixtures, and hence desire the processing capability of arbitrary frequency bands. Emulating some form of agility in RF electronics requires large banks of sub-circuits (each designed for a specific frequency band) for a broad spectrum coverage [7], and sophisticated switching technology to ensure smooth transitions across frequency bands [8]. These practical difficulties pose serious challenges to meeting the future needs of radio spectrum access, and motivate the development of RF photonics that provides a completely different set of signal processing properties [9].

In an RF photonic receiver, the input RF signal modulates the intensity of an optical carrier [i.e., electrical-to-optical (E/O) conversion], which is then detected to yield the output RF signal [i.e., optical-to-electrical (O/E) conversion] [10]. By effectively upconverting to a 193 THz intermediate frequency, photonic processors are nearly frequency independent: even gigahertz signals are considered narrowband on the optical spectrum because fibers/waveguides hold a flat frequency response over a 5 THz window [11]. Between E/O modulation and O/E detection, optical signals can be processed with tunable optical devices, which may benefit from both the unconventional utilization of

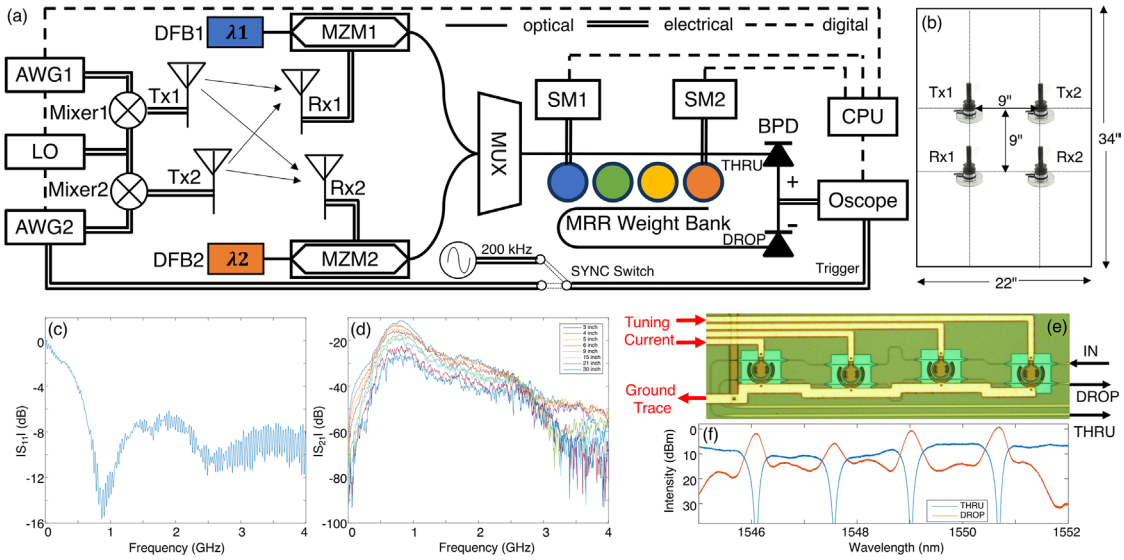

Fig. 1. (a) Schematic illustration of the experimental setup for photonic BSS. DFB, distributed feedback laser; MZM, Mach–Zehnder modulator; AWG, arbitrary wave generator; LO, local oscillator; Tx, transmitting antenna; Rx, receiving antenna; MUX, WDM multiplexer; SM, source meter; BPD, balanced photo-detector; Oscope, sampling oscilloscope. The synchronization (SYNC) switch toggles the Oscope triggering state between a repeating pattern from AWGs and a free-running clock at 200 kHz. (b) Configuration of antennas for photonic BSS experiment. (c) S_{11} measurement of a single antenna. (d) S_{21} measurement between two antennas. (e) Zoomed-in micrograph of the MRR weight bank cascading four MRRs in a parallel add/drop configuration. Each MRR has a dedicated metal trace to adjust individual resonance condition through thermal tuning, but shares the same ground trace to reduce the electrical I/O count. (f) Spectral response of the MRR weight bank measured from both the THRU and DROP ports.

standard photonic integrated devices for linear analog computation, and the enormous information density made possible through wavelength-division multiplexing (WDM) [12].

In this work, we report the first conceptual proposal and experimental demonstration of photonic BSS. From the perspective of hardware design, our scheme introduces frequency independence through the addition of an RF photonic front-end, which converts RF mixtures to WDM signals regardless of their frequency bands. This RF photonic front-end also implements a parallel matrix-vector multiplication operation called weighted addition, which projects the multi-dimensional WDM signals onto a salient, few-dimensional representation. Essentially, this is achieved by a single on-chip microring resonator (MRR) weight bank carrying out channel-wise weighting (i.e., spectral filtering) on an individual WDM signal followed by a balanced photo-detector (BPD) producing their summation [13]. From the perspective of a control algorithm, our scheme integrates our prior experience on photonic principal component analysis (PCA) [14] and photonic independent component analysis (ICA) [15], which together constitute a two-step procedure for a complete photonic BSS pipeline. The novelty of such a pipeline lies in the fact that it entails no explicit waveform information from mixtures; instead, it synthesizes univariate statistics from the reduced dimensional output of the RF photonic front-end to reconstruct the multivariate statistics required for BSS.

Figure 1(a) shows the experimental setup of photonic BSS. We employ two arbitrary waveform generators (AWGs, Agilent 33220A) as the independent sources in this two-channel photonic BSS experiment. We program one AWG to generate a baseband signal using binary phase-shift keying (BPSK), and the other one to generate a baseband signal using amplitude-shift keying (ASK). Both baseband signals are upconverted to RF frequency at two mixers that share the same local oscillator (LO, Rohde & Schwarz SMBV100A). Two transmitting antennas, Tx1, Tx2, deliver the RF signals to two receiving antennas, Rx1, Rx2, over the air, where an unknown mixing process occurs [Fig. 1(b)]. All these four omnidirectional antennas are of the same model (L-com HG2403U-NMO). Their S11 measurement is shown in Fig. 1(c), while the S21 measurement between two antennas separated by different distances is shown in Fig. 1(d). Both figures suggest these antennas have a minimum loss for frequency bands around 900 MHz.

A hybrid analog–digital platform is built to receive and process mixtures for photonic BSS, featuring an RF photonic front-end aided by a digital signal processing (DSP) back-end. Two distributed feedback lasers (DFBs) are used to generate optical carriers at 1546.92 nm and 1551.72 nm. Each optical carrier is modulated at a Mach–Zehnder modulator (MZM) by the RF signal received from either Rx1 or Rx2, and multiplexed together at a WDM multiplexer (MUX). The WDM signals then couple into a silicon photonic chip mounted on a temperature-controlled fiber alignment stage (see [14,15] for details on chip fabrications and characterizations). The chip contains an MRR weight bank, as shown in Fig. 1(e), which directs WDM signals from the IN port to the THRU and DROP ports in a controllable ratio depending on the resonance condition of individual wavelengths with the corresponding MRR.

In this work, we employ those two MRRs whose resonance positions are located at 1546.08 nm and 1550.69 nm [see Fig. 1(f) for the spectral response of the MRR weight bank]. Each MRR is driven by a source meter (SM, Keithley 2400) set in current-source, voltage-measure mode. In-ring photoconductive heaters are implemented to enable thermal tuning and feedback control on the MRR weight bank [16]. As in our prior works [14,15], we perform MRR weight bank calibration to obtain a robust mapping between sourced currents and achieved weights, and ensure at least five bits of weight accuracy and precision before applying it for photonic BSS experiments. The

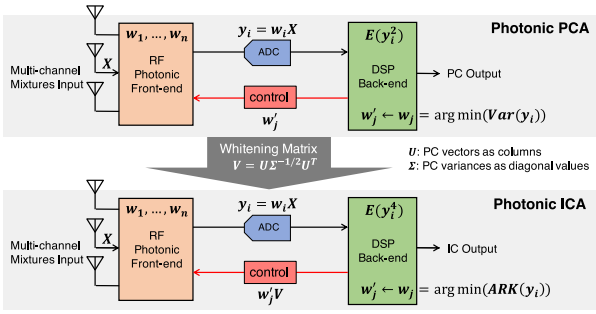

Fig. 2. Two-step photonic BSS pipeline leveraging the hybrid analog–digital platform consisting of an RF photonic front-end and a DSP back-end. The DSP back-end executes photonic PCA and photonic ICA procedures based solely on reduced dimensional statistics observed from the weighted addition output of RF photonic front-end.

outputs at THRU and DROP ports are summed off-chip by a BPD (Discovery Semiconductors DSC-R405ER), and the resulted weighted addition output is recorded by a sampling oscilloscope (Oscope, Tektronix DSA8300). AWGs, Oscope, and SMs are computer-controlled by *lightlab* software [17].

We further utilize a synchronization (SYNC) switch to swap between two triggering conditions for the Oscope, following the practice of multivariate photonics assuming the waveform information may not be readily available in real-life BSS scenarios (simply cannot guarantee sampling above the Nyquist rate of an unknown frequency band) [18]. We emulate such constrained observability by triggering the Oscope in free-running mode with its internal clock of 200 kHz, under which circumstance the signal can be sampled only at a sub-Nyquist rate (200 kS/s here). Occasionally when the waveform information is needed (e.g., for performance evaluation), the Oscope can be triggered in synchronized mode with the AWGs to synthesize the accurate waveform at a super-Nyquist sampling rate (16 GS/s here).

The above constrained observability also motivates the development of a two-step photonic BSS pipeline shown in Fig. 2, which is based on close interactions between RF photonic front-end and DSP back-end. We frame the photonic BSS pipeline as a variate of projection pursuit [19] by initializing multiple (normalized) weight vectors $w_i (i = 1, \ldots, n)$ at (the MRR weight bank of) the RF photonic front-end. Upon receiving the multi-channel mixtures input X, the RF photonic front-end projects it onto the subspace of $w_i (i = 1, \ldots, n)$ by producing the reduced dimensional weighted addition output $y = w_i X (i = 1, \ldots, n)$ without discrimination against its frequency band. The DSP back-end, on the other hand, controls the way the RF photonic front-end projects mixtures input by updating the weight vectors based on control algorithms discussed below.

In the first step, photonic PCA updates the weight vectors to converge at the target PC vectors by maximizing the variance (Var) of weighted addition output $E(y_i^2)$ [14]. Performing photonic PCA in the first place is useful, as its outcomes (i.e., PC vectors and variances) can be used to construct a specialized matrix called a whitening matrix, which may reduce the BSS problem to finding an orthogonal transformation (rather than the inverse matrix of a mixing matrix) [19]. In the second step, photonic ICA takes as argument this whitening matrix V, and updates the weight vectors in the whitened subspace $w_i V (i = 1, \ldots, n)$ to converge at the target IC vectors by maximizing the absolute relative kurtosis (ARK) of weighted addition output against Gaussian distribution $|E(y_i^4)/\sigma^4(y_i) - 3|$ (σ^2 is variance) [15]. Here, photonic ICA draws inspiration from the central limit theorem that the true sources are supposed to maximize their non-Gaussianity (relative distance from the Gaussian distribution).

Our customized photonic BSS pipeline is viable without explicit waveform digitization, but requires only the second-order and fourth-order statistics from the reduced dimensional weighted addition output. In contrast, conventional BSS solutions (e.g., FastICA [20]) require capturing the complete waveform information of mixtures, which is generally not applicable to multi-band BSS unless their Nyquist rates can be obtained in advance. In this work, we intentionally make this condition hold to implement FastICA for comparison, such that it not only validates the correctness of photonic BSS but also shows photonic BSS may achieve separation performance close to digital-software BSS estimations.

Figure 3 presents the experimental results of two-channel multi-band photonic BSS where we first run the photonic BSS pipeline to find the PC/IC vectors in free-running mode, and then apply them at the RF photonic front-end to obtain the waveforms of estimated sources in synchronized mode (for evaluation). The band whose central frequency is at 880 MHz [Fig. 3(b)] exhibits relatively clean mixtures (blue curves in left column) and source separations (red curves in right column), which can be attributed to the fact that antennas hold the best transmission window around 900 MHz. The top mixture (RX1) is received by the antenna that is closer to the BPSK transmitter, while the bottom mixture (RX2) is received by the antenna that is closer to the ASK transmitter. The photonic BSS pipeline demonstrates its effectiveness by successfully separating these two sources, resulting in the top estimated source (IC1) being the BPSK (cannot tell zeros and ones from its intensity) and the bottom estimated source (IC2) being the ASK (zeros are at the ground level, while ones are represented by those envelopes). The other two bands whose central frequencies are at 781 MHz [Fig. 3(a)] and 1000 MHz [Fig. 3(c)] experience more difficulty of accurate source estimation caused by higher signal-to-noise in received mixtures, though they still manage to achieve perceivably effective source separation.

Figure 4 summarizes quantitative photonic BSS performance over 15 frequency bands (listed in the table on the right). For each frequency band, we run the photonic BSS pipeline six times to acquire (a) the average root-mean-squared error (RMSE) between estimated and ground-truth sources among all runs to quantify accuracy, and (b) the standard deviation (SD) of estimated sources among all runs to quantify repeatability. The tested frequency bands cover a spectrum range of about 400 MHz. The major bottleneck lies in RF components (i.e., antennas in this work) whose operating bandwidth strictly limits the frequency agility of photonic BSS demonstrated here. Those frequency bands in the vicinity of 900 MHz exhibit uniformly good performance with no more than 20% RMSEs for both estimated sources. Those frequency bands at the two ends of the antenna optimal transmission window show comparatively worse performance with up to 50% RMSEs, though such degradation results mainly from the limitation of RF components rather than photonics. All frequency bands express less than 5% SDs (error bars) in their estimated sources.

In conclusion, the unprecedented tunability across a spectrum makes RF photonics an attractive alternative to RF

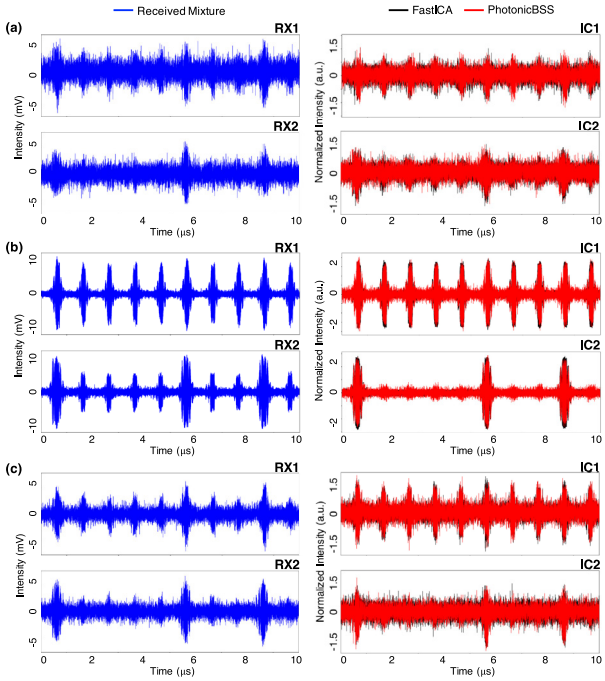

Fig. 3. Experimental waveforms of the received mixtures (left column) and corresponding estimated sources (right column) when performing FastICA (black) and photonic BSS (red) at three frequency bands whose central frequencies are at: (a) 781 MHz, (b) 880 MHz, and (c) 1000 MHz.

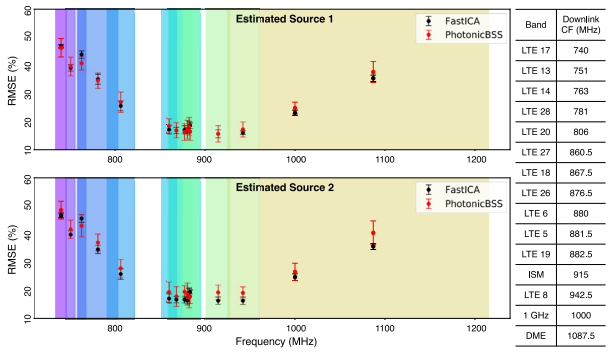

Band	Downlink CF (MHz)
LTE 17	740
LTE 13	751
LTE 14	763
LTE 28	781
LTE 20	806
LTE 27	860.5
LTE 18	867.5
LTE 26	876.5
LTE 6	880
LTE 5	881.5
LTE 19	882.5
ISM	915
LTE 8	942.5
1 GHz	1000
DME	1087.5

Fig. 4. Experimental demonstration of photonic BSS (red) over multiple frequency bands (each represented by one color strip), including 12 long-term evolution (LTE) bands, an industrial, scientific, and medical (ISM) band, a 1 GHz band, and a distance measuring equipment (DME) band. The downlink central frequencies of these bands (table on the right) are set as the RF carrier frequency at the local oscillator. The FastICA results (black) are provided for reference.

electronics to address the BSS problem at the forefront of cellular networks. We propose and demonstrate photonic BSS adopting an RF photonic front-end to process and demix RF signals in a single piece of on-chip MRR weight bank, enabling true blindness with respect to the operating bandwidth of received mixtures. We also contribute a photonic BSS pipeline treating the waveform information of mixtures as redundancy, but requiring only certain statistical information of the reduced dimensional weighted addition output from the RF photonic front-end. We perform the first proof-of-concept photonic BSS experiments where we test the proposed approach on mixed-over-the-air RF signals at 15 frequency bands across approximately 400 MHz range.

This work can be significantly extended in multiple aspects. For example, RF components upgrade may potentially increase the spectral tuning distance up to gigahertz range, though the cost can be considerable in terms of matching wideband devices across sources, filters, mixers, splitters, antennas, etc. Future research may also consider more diversified source characteristics and longer transmission distances for broader applications of the proposed technique. Another promising direction is to generalize photonic BSS to higher dimensions, as we restrict this work to two-channel, given the implementation cost that the number of discrete DFBs, MZMs, and SMs all scale linearly with the number of channels. A tentative solution exists with larger-scale integration efforts aiming to integrate every component aforementioned onto the same substrate [21].

Funding. Defense Advanced Research Projects Agency (HR-00111990049); National Science Foundation (ECCS-1642962).

Disclosures. The authors declare no conflicts of interest.

REFERENCES

1. I. F. Akyildiz, W. Y. Lee, M. C. Vuran, and S. Mohanty, Comput. Netw. **50**, 2127 (2006).
2. V. Venkateswaran and A. J. van der Veen, IEEE Trans. Signal Process. **58**, 4131 (2010).
3. S. Haykin, IEEE J. Sel. Areas Commun. **23**, 201 (2005).
4. S. Choi, A. Cichocki, H. M. Park, and S. Y. Lee, Neural Inf. Process. Lett. Rev. **6**, 1 (2005).
5. T. H. Lee, *The Design of CMOS Radio-frequency Integrated Circuits* (Cambridge University, 2003).
6. R. Mongia, I. J. Bahl, and P. Bhartia, *RF and Microwave Coupled-line Circuits* (Artech house, 1999).
7. E. Lourandakis, R. Weigel, H. Mextorf, and R. Knoechel, IEEE Microw. Mag. **13**(1), 111 (2012).
8. Skyworks Solutions, Inc., "Choosing the right RF switches for smart mobile device applications," White Paper (2011).
9. J. Capmany, J. Mora, I. Gasulla, J. Sancho, J. Lloret, and S. Sales, J. Lightwave Technol. **31**, 571 (2013).
10. D. Marpaung, C. Roeloffzen, R. Heideman, A. Leinse, S. Sales, and J. Capmany, Laser Photon. Rev. **7**, 506 (2013).
11. G. P. Agrawal, *Fiber-optic Communication System* (Wiley, 2002).
12. P. R. Prucnal and B. J. Shastri, *Neuromorphic Photonics* (CRC Press, 2017).
13. A. N. Tait, A. X. Wu, T. F. de Lima, E. Zhou, B. J. Shastri, M. A. Nahmias, and P. R. Prucnal, IEEE J. Sel. Top. Quantum Electron. **22**, 312 (2016).
14. P. Y. Ma, A. N. Tait, T. F. De Lima, S. Abbaslou, B. J. Shastri, and P. R. Prucnal, Opt. Express **27**, 18329 (2019).
15. P. Y. Ma, A. N. Tait, T. F. de Lima, C. Huang, B. J. Shastri, and P. R. Prucnal, Opt. Express **28**, 1827 (2020).
16. A. N. Tait, H. Jayatilleka, T. F. D. Lima, P. Y. Ma, M. A. Nahmias, B. J. Shastri, S. Shekhar, L. Chrostowski, and P. R. Prucnal, Opt. Express **26**, 26422 (2018).
17. A. Tait, T. Ferreira de Lima, P. Y. Ma, Z. Guo, A. Jha, H.-T. Peng, and H. Miller, lightwave-lab/lightlab: Version 1.0.7 (2019).
18. A. N. Tait, P. Y. Ma, T. F. De Lima, E. C. Blow, M. P. Chang, M. A. Nahmias, B. J. Shastri, and P. R. Prucnal, J. Lightwave Technol. **37**, 5996 (2019).
19. A. Hyvärinen and E. Oja, Neural Netw. **13**, 411 (2000).
20. A. Hyvärinen, IEEE Trans. Neural Netw. **10**, 626 (1999).
21. M. J. Heck, J. F. Bauters, M. L. Davenport, J. K. Doylend, S. Jain, G. Kurczveil, S. Srinivasan, Y. Tang, and J. E. Bowers, IEEE J. Sel. Top. Quantum Electron. **19**, 6100117 (2013).